An Improved FB/NSA Algorithm for the Computation of Scattering from Two-Dimensional Large-Scale Rough Surfaces

D. Torrungrueng and Joel T. Johnson

The Ohio State University

Department of Electrical Engineering

ElectroScience Laboratory

1320 Kinnear Road, Columbus, Ohio 43212

Tel: (614)292-7981, Fax: (614)292-7297

torrungd@ee.eng.ohio-state.edu

johnson@ee.eng.ohio-state.edu

Abstract:

The forward-backward method with a novel spectral acceleration algorithm (FB/NSA) has been shown to be a very efficient $\mathcal{O}(N_{tot})$ iterative method of moments, where N_{tot} is the total number of unknowns to be solved, for the computation of electromagnetic wave scattering from two-dimensional (2-D) rough surfaces (3-D scattering problems). For *relatively large* surface cross-range sizes D_y, the method's efficiency decreases due to the increase of the direct computation of the mutual coupling in the strong region. An additional NSA formulation based on spectral domain representation of the Green's function in the cross-range direction is incorporated into the standard NSA algorithm to improve its computational efficiency. In addition, for the case of *extremely* large-scale rough surfaces, a "multilevel" algorithm (i.e. decomposing 2-D *extremely* large-scale surfaces into more than one weak region and appropriately choosing the NSA parameters for each weak region) is incorporated into the standard FB/NSA algorithm to improve its accuracy. It is found that the improved FB/NSA algorithm remains $\mathcal{O}(N_{tot})$. Numerical results show that the efficiency and accuracy of the standard FB/NSA algorithm are improved by incorporating the y- expansion and the "multilevel" algorithm at the cost of increasing algorithmic complexity and memory requirements.

1 Introduction

The forward-backward method with a novel spectral acceleration algorithm (FB/NSA) has been shown to be a very efficient $\mathcal{O}(N_{tot})$ iterative method of moments, where N_{tot} is the total number of unknowns to be solved, for the computation of electromagnetic wave scattering from two-dimensional (2-D) rough surfaces (3-D scattering problems) [1, 2]. In the FB/NSA method, a neighborhood distance in the along-range direction around each receiving element on the surface is defined to separate the strong interaction region from the weak interaction region. Direct matrix-vector multiplication is performed when the source points are in the strong interaction region, and the NSA algorithm is employed to rapidly compute interactions between widely separated points in the conventional FB method. The NSA algorithm involves a *double* spectral integral representation of source currents and the 3-D free space scalar Green's function in the along-range direction. Efficiency improvements of the FB/NSA algorithm for 2-D surfaces (compared to the conventional FB method) are appreciable but not as dramatic as those for 1-D surfaces. However, for a fixed surface cross-range size D_y the computational efficiency of the 2-D FB/NSA method remains $\mathcal{O}(N_{tot})$ as the surface down-range size D_x increases. In addition, the 2-D FB/NSA method is specifically designed for 2-D large-scale finite rectangular surfaces and remains very efficient for moderately-rough large-scale surfaces [3]. Use of a large rectangular surface makes the method well suited for studying rough surface scattering at low grazing angles (LGA).

For *relatively large* surface cross-range sizes D_y, the efficiency of the 2-D FB/NSA method decreases due to the increase of the direct computation of the mutual coupling in the strong region. One way to improve the computational efficiency of the strong-region computation is to incorporate an additional NSA formulation based on the spectral domain representation of the Green's function in the y- direction. In addition, as in the case of 1-D surfaces [4], the 2-D FB/NSA algorithm with only one large weak region may yield inaccurate results for *extremely* large-scale rough surfaces. Inaccuracy comes from the fact that the complex vector radiation function of a source group far separated from the receiving element is *rapidly decayed* along the deformed contours away from the origin in the complex planes. A "multilevel" algorithm for 2-D *extremely* large-scale rough surfaces analogous to that for the 1-D case is proposed to solve this problem. Numerical results show that

the efficiency and accuracy of the standard FB/NSA algorithm are improved by incorporating the y- expansion and the "multilevel" algorithm at the cost of increasing algorithmic complexity and memory requirements.

This paper is organized as follows. Section 2 presents the formulation of the 2-D FB/NSA algorithm, using spectral domain representation of the Green's function in the x- and y- directions, for the computation of scattering from 2-D perfect electric conducting (PEC) rough surfaces. The "multilevel" FB/NSA algorithm for 2-D *extremely* large-scale PEC rough surfaces is discussed in Section 3. Section 4 discusses the computational cost and memory storage requirements of the improved 2-D FB/NSA method. Numerical results are presented in Section 5, and conclusions can be found in Section 6. An $e^{-i\omega t}$ time-harmonic convention is assumed and suppressed throughout this paper, and the propagation constant is defined as $k = \omega\sqrt{\mu\epsilon}$, where ω is the radian frequency and ϵ and μ are the permittivity and permeability of free space, respectively.

2 Formulation of the 2-D FB/NSA Algorithm Using Spectral Domain Representation of the Green's Function in the x- and y- Directions

Consider a 2-D PEC rough surface profile S illuminated by an incident field $\mathbf{E}^i(x, y, z)$ centered in direction $\hat{k}_i = \hat{x}\sin\theta_i\cos\phi_i + \hat{y}\sin\theta_i\sin\phi_i - \hat{z}\cos\theta_i$, as shown in Figure 1, where θ_i and ϕ_i refer to the incident polar and azimuthal angles, respectively. The region above the surface profile is assumed to be free space. The surface height function $z = f(x, y)$ has zero mean and its maximum and minimum height variations are denoted by z_{max} and z_{min}, respectively. Let Δz_{max} denote the largest surface variation, which is equal to $z_{max} - z_{min}$. The incident field $\mathbf{E}^i(x, y, z)$ is tapered with a Gaussian beam amplitude pattern confining the illuminated rough surface to the rectangular surface area $D_x \times D_y$ so that surface edges do not contribute strongly to obtained scattered fields. The tapered incident field is discussed in detail in [3]–[6].

Let $\mathbf{r} = \hat{x}x + \hat{y}y + \hat{z}z$ and $\mathbf{r}\prime = \hat{x}x\prime + \hat{y}y\prime + \hat{z}z\prime$ denote a field point and a source point on the rough surface, respectively. Then, the magnetic field integral equation (MFIE) on the PEC rough

surface is given by

$$\mathbf{J}(\mathbf{r}) = \mathbf{J}_{PO}(\mathbf{r}) + 2\,\mathbf{n} \times \iint_{PV,S_{xy}} dx\prime\, dy\prime \nabla g(\mathbf{r},\mathbf{r}\prime) \times \mathbf{J}(\mathbf{r}\prime), \tag{1}$$

where the above integral is a principal-value integral,

$$g(\mathbf{r},\mathbf{r}\prime) = \frac{e^{ikR}}{4\pi R} \tag{2}$$

$$\nabla g(\mathbf{r},\mathbf{r}\prime) = G(R)\mathbf{R} \tag{3}$$

$$G(R) = \frac{e^{ikR}}{4\pi R^2}\left(ik - \frac{1}{R}\right), \tag{4}$$

∇ denotes the gradient operator in the three-dimensional coordinate system, $\mathbf{J}(\mathbf{r}) = \mathbf{n} \times \mathbf{H}(\mathbf{r})$, $\mathbf{J}_{PO}(\mathbf{r}) = 2\mathbf{n} \times \mathbf{H}^i(\mathbf{r})$, $\mathbf{n} = \hat{z} - \hat{x}\frac{\partial f}{\partial x} - \hat{y}\frac{\partial f}{\partial y}$, $\mathbf{R} = \mathbf{r} - \mathbf{r}\prime$ and $R = |\mathbf{R}|$, , where $\mathbf{H}^i$ is the incident magnetic field associated with $\mathbf{E}^i$. The normal vector $\mathbf{n}$ (not a unit vector) points upward from the PEC surface and S_{xy} is the surface obtained from the projection of the rough surface S onto the $x - y$ plane. As usual, this surface integral equation can be solved using a standard point-matching MM technique [7]. For the purpose of the MM formulation, the rectangular surface area $D_x \times D_y$ of S_{xy} is discretized into the $N \times M$ rectangular grid. Each element has the dimension $\Delta x \times \Delta y$, where $\Delta x = \frac{D_x}{N}$ and $\Delta y = \frac{D_y}{M}$. Let $N_{tot} = 2NM$ be the total number of unknowns on the surface S (due to 2 independent vector components for $\mathbf{J}(\mathbf{r})$).

In the 2-D FB method, the current vector $\mathbf{J}(\mathbf{r})$ is decomposed into the the forward-stepping (FS) $\mathbf{J}^f(\mathbf{r})$ and backward-stepping (BS) $\mathbf{J}^b(\mathbf{r})$ currents as follows:

$$\mathbf{J}(\mathbf{r}) = \mathbf{J}^f(\mathbf{r}) + \mathbf{J}^b(\mathbf{r}). \tag{5}$$

The FS and BS processes are shown in Figure 3 in [1]. The detail of the 2-D FB method can be found in [1]. For convenience in understanding the 2-D NSA algorithm, the computation of the FS process is considered only; the BS computation can also be treated in a similar fashion. The *original* 2-D NSA algorithm [1] starts with selection of a neighborhood distance in the x- direction, L_x, within which interactions between points are classified as strong and outside of which interactions are classified as weak, as illustrated in Figure 2. It can be seen that the FS surface S_{xy}^f is decomposed into the FS strong ($S_{xy,s}^f$) and weak ($S_{xy,w}^f$) regions. In the strong region, the FS current is computed in the conventional manner, and the NSA algorithm is employed to compute the FS current in the

weak region. The original 2-D NSA algorithm is based on the spectral domain representation of the free space 3-D scalar Green's function in the x- direction, and it is discussed in detail in [1].

For *relatively large* surface cross-range sizes D_y, the efficiency of the original 2-D NSA algorithm decreases due to the increase of the direct computation of the mutual coupling in the strong region. One way to improve its computational efficiency of the strong-region computation is to incorporate an additional NSA formulation based on the spectral domain representation of the Green's function in the y- direction. As shown in Figure 3, the strong region contribution to the FS current on the kth iteration $\mathbf{J}_s^{f,(k)}(\mathbf{r})$ can be written as follows:

$$\mathbf{J}_s^{f,(k)}(\mathbf{r}) \; = \; 2\,\mathbf{n} \times \iint_{PV, S_{xy,s}^f} dx\prime\, dy\prime\, G(R)\, \mathbf{R} \times \left[\mathbf{J}^{f,(k)}(\mathbf{r}\prime) + \mathbf{J}^{b,(k-1)}(\mathbf{r}\prime) \right] \tag{6}$$

$$= \; \mathbf{J}_{rs}^{f,(k)}(\mathbf{r}) + \mathbf{J}_{w,yt}^{f,(k)}(\mathbf{r}) + \mathbf{J}_{w,yb}^{f,(k)}(\mathbf{r}), \tag{7}$$

where

$$\mathbf{J}_{rs}^{f,(k)}(\mathbf{r}) \; = \; 2\,\mathbf{n} \times \iint_{PV, S_{xy,rs}^f} dx\prime\, dy\prime\, G(R)\, \mathbf{R} \times \left[\mathbf{J}^{f,(k)}(\mathbf{r}\prime) + \mathbf{J}^{b,(k-1)}(\mathbf{r}\prime) \right] \tag{8}$$

$$\mathbf{J}_{w,yt}^{f,(k)}(\mathbf{r}) \; = \; 2\,\mathbf{n} \times \iint_{S_{xy,yt}^f} dx\prime\, dy\prime\, \nabla g(\mathbf{r},\mathbf{r}\prime) \times \left[\mathbf{J}^{f,(k)}(\mathbf{r}\prime) + \mathbf{J}^{b,(k-1)}(\mathbf{r}\prime) \right] \tag{9}$$

$$\mathbf{J}_{w,yb}^{f,(k)}(\mathbf{r}) \; = \; 2\,\mathbf{n} \times \iint_{S_{xy,yb}^f} dx\prime\, dy\prime\, \nabla g(\mathbf{r},\mathbf{r}\prime) \times \left[\mathbf{J}^{f,(k)}(\mathbf{r}\prime) + \mathbf{J}^{b,(k-1)}(\mathbf{r}\prime) \right], \tag{10}$$

and $S_{xy,s}^f = S_{xy,rs}^f + S_{xy,yt}^f + S_{xy,yb}^f$. The terms $\mathbf{J}_{rs}^{f,(k)}(\mathbf{r}), \mathbf{J}_{w,yt}^{f,(k)}(\mathbf{r})$ and $\mathbf{J}_{w,yb}^{f,(k)}(\mathbf{r})$ in Eq. (6) represent the *new* strong region contribution, and the weak region contributions using the spectral domain representation in the y- direction for $y < y\prime$ and $y > y\prime$, respectively. Note that the term $\mathbf{J}_{rs}^{f,(k)}(\mathbf{r})$ is computed in the conventional manner, and the NSA algorithm is employed to compute the terms $\mathbf{J}_{w,yt}^{f,(k)}(\mathbf{r})$ and $\mathbf{J}_{w,yb}^{f,(k)}(\mathbf{r})$. Let L_y be a neighborhood distance in the y- direction as illustrated in Figure 3. Note that the size of the strong region $S_{xy,s}^f$ is reduced to $S_{xy,rs}^f$ of approximate size $L_x \times 2L_y$; i.e. the reduction of the direct computation, but the complexity of the NSA algorithm increases. Thus, a neighborhood distance L_y must be chosen appropriately to compromise between the direct computation of $\mathbf{J}_{rs}^{f,(k)}(\mathbf{r})$ and the NSA computation of $\mathbf{J}_{w,yt}^{f,(k)}(\mathbf{r})$ and $\mathbf{J}_{w,yb}^{f,(k)}(\mathbf{r})$.

To illustrate the 2-D FB/NSA algorithm using both x- and y- expansions, consider the FS process as shown in Figure 4 for a *simple* configuration with the following parameters: $N = 5, M = 5, N_x = 3$ and $N_y = 2$, where $N_x = \frac{L_x}{\Delta x}$ and $N_y = \frac{L_y}{\Delta y}$. The FS process starts from Figure 4 (a) and ends with Figure 4 (y). Note that the receiving element moves from bottom to top, and then from

left to right. In addition, the *weak* region employing the NSA algorithm with the x- expansion is the same as shown in Figure 2, and only the *old* strong region is modified. Thus, it is sufficient to consider only the FS process when the receiving element moves in the *vertical* direction; i.e. consider along a *column* instead of a *row*. Without loss of generality, it is convenient to consider only the "middle" column of Figure 4; i.e. Figures 4 (k) to 4 (o). When the receiving element is located at the bottom as shown in Figure 4 (k), only the regions $S_{xy,rs}^f$ (which employs direct computation) and $S_{xy,yt}^f$ (which applies the NSA algorithm with the y- direction for $y < y\prime$) contribute. Note that there is no region $S_{xy,yb}^f$ employing the NSA algorithm with the y- direction for $y > y\prime$ in Figure 4 (k). As the receiving element moves upward, the region $S_{xy,yt}^f$ decreases, but the region $S_{xy,yb}^f$ increases. Note that the region $S_{xy,rs}^f$ tends to maintain the same size except when the receiving element is near the bottom or the top. Finally, as the receiving element approaches the top (see Figures 4 (n) and 4 (o)), there are only the regions $S_{xy,rs}^f$ and $S_{xy,yb}^f$; i.e. the region $S_{xy,yt}^f$ vanishes. Next, consider the formulation of the 2-D FB/NSA algorithm using the y- expansion in detail.

Without loss of generality, only the term $\mathbf{J}_{w,yb}^{f,(k)}(\mathbf{r})$ associated with the spectral domain representation in the y- direction for $y > y\prime$ is considered. The term $\mathbf{J}_{w,yt}^{f,(k)}(\mathbf{r})$ for $y < y\prime$ can be formulated in a similar fashion, except for minor changes as will be discussed later in this section. The NSA algorithm associated with $\mathbf{J}_{w,yb}^{f,(k)}(\mathbf{r})$ starts with the spectral integral representation of the Green's function $g(\mathbf{r},\mathbf{r}\prime)$ and $\nabla g(\mathbf{r},\mathbf{r}\prime)$ propagating in the y- direction for $y - y\prime > 0$ as follows:

$$g(\mathbf{r},\mathbf{r}\prime) \quad = \quad \frac{i}{8\pi^2} \int_{C_{k_z}} \int_{C_{k_x}} dk_z \, dk_x \, \frac{e^{i\mathbf{k}\cdot\mathbf{R}}}{k_y} \tag{11}$$

$$\nabla g(\mathbf{r},\mathbf{r}\prime) \quad = \quad -\frac{1}{8\pi^2} \int_{C_{k_z}} \int_{C_{k_x}} dk_z \, dk_x \, \frac{\mathbf{k}e^{i\mathbf{k}\cdot\mathbf{R}}}{k_y}, \tag{12}$$

where $\mathbf{k} = \hat{x}k_x + \hat{y}k_y + \hat{z}k_z$ and $k_y = (k^2 - k_x^2 - k_z^2)^{\frac{1}{2}}$. The contours C_{k_z} and C_{k_x} are the *original* contours of integration on the entire real axis starting from $-\infty$ to ∞ in the complex k_z and k_x planes, respectively. Substituting Eq. (12) into Eq. (10) and interchanging the spatial and contour integrations, Eq. (10) can be rewritten as follows:

$$\mathbf{J}_{w,yb}^{f,(k)}(\mathbf{r}) \quad = \quad -\frac{1}{4\pi^2} \, \mathbf{n} \times \int_{C_{k_z}} \int_{C_{k_x}} dk_z \, dk_x \, \frac{\mathbf{F}_{yb}^{(k)}(\mathbf{r}, k_z, k_x)}{k_y} \tag{13}$$

$$\mathbf{F}_{yb}^{(k)}(\mathbf{r}, k_z, k_x) \quad = \quad \iint_{S_{xy,yb}^f} dx\prime \, dy\prime \, \mathbf{V}_{yb}^{(k)}(\mathbf{r}\prime) \, e^{i\mathbf{k}\cdot\mathbf{R}}, \tag{14}$$

7

where $\mathbf{V}_{yb}^{(k)}(\mathbf{r}\prime)$ is defined as

$$\mathbf{V}_{yb}^{(k)}(\mathbf{r}\prime) = \mathbf{k} \times \left[\mathbf{J}^{f,(k)}(\mathbf{r}\prime) + \mathbf{J}^{b,(k-1)}(\mathbf{r}\prime) \right]. \tag{15}$$

As in the case of the x- expansion, the discretized version of the complex vector radiation function $\mathbf{F}_{yb}^{(k)}(\mathbf{r}_{(n,m)}, k_z, k_x)$ can be computed from currents in the region $S_{xy,yb}^{f}$ in a *recursive* manner through a "phase shifting" process, where $\mathbf{r}_{(n,m)}$ denotes a position vector starting from the origin of the coordinate system to the center of (n, m) th element on the surface S. To see this, first consider the region $S_{xy,yb}^{f}$ when the receiving element moves in the *vertical* direction. The radiation function $\mathbf{F}_{yb}^{(k)}(\mathbf{r}_{(n,m)}, k_z, k_x)$ can be computed numerically as follows. For $1 \leq m \leq N_y$, where $N_y = \frac{L_y}{\Delta y}$,

$$\mathbf{F}_{yb}^{(k)}(\mathbf{r}_{(n,m)}, k_z, k_x) = \mathbf{0} \tag{16}$$

since the weak region $S_{xy,yb}^{f}$ does not exist. For $m > N_y$; i.e. the weak region $S_{xy,yb}^{f}$ exists,

$$\mathbf{F}_{yb}^{(k)}(\mathbf{r}_{(n,m)}, k_z, k_x) = \begin{cases} \mathbf{F}_{1}^{(k)}(\mathbf{r}_{(n,m)}, k_z, k_x) & , n = 1 \\ \mathbf{F}_{2}^{(k)}(\mathbf{r}_{(n,m)}, k_z, k_x) & , 1 < n \leq N_x \\ \mathbf{F}_{3}^{(k)}(\mathbf{r}_{(n,m)}, k_z, k_x) & , n > N_x \end{cases} \tag{17}$$

where

$$\mathbf{F}_{1}^{(k)}(\mathbf{r}_{(n,m)}, k_z, k_x) = \begin{cases} \mathbf{0} & , m \leq N_y \\ \mathbf{F}_{1}^{(k)}(\mathbf{r}_{(n,m-1)}, k_z, k_x) \, e^{i\Psi_{yb,1}} + \mathbf{F}_{1,add}^{(k)} & , m > N_y \end{cases} \tag{18}$$

$$\mathbf{F}_{2}^{(k)}(\mathbf{r}_{(n,m)}, k_z, k_x) = \mathbf{F}_{yb}^{(k)}(\mathbf{r}_{(n-1,m)}, k_z, k_x) \, e^{i\Psi_{yb,2}} + \mathbf{F}_{1}^{(k)}(\mathbf{r}_{(n,m)}, k_z, k_x) \tag{19}$$

$$\mathbf{F}_{3}^{(k)}(\mathbf{r}_{(n,m)}, k_z, k_x) = \left[\mathbf{F}_{yb}^{(k)}(\mathbf{r}_{(n-1,m)}, k_z, k_x) - \mathbf{F}_{4}^{(k)}(\mathbf{r}_{(n-1,m)}, k_z, k_x) \right] \cdot$$
$$e^{i\Psi_{yb,2}} + \mathbf{F}_{1}^{(k)}(\mathbf{r}_{(n,m)}, k_z, k_x), \tag{20}$$

and

$$\mathbf{F}_{4}^{(k)}(\mathbf{r}_{(n-1,m)}, k_z, k_x) = \begin{cases} \mathbf{0} & , m \leq N_y \\ \mathbf{F}_{4}^{(k)}(\mathbf{r}_{(n-1,m-1)}, k_z, k_x) \, e^{i\Psi_{yb,3}} \\ + \mathbf{F}_{4,add}^{(k)} & , m > N_y \end{cases} \tag{21}$$

$$\mathbf{F}_{1,add}^{(k)} = \Delta S_{xy} \mathbf{V}_{yb}^{(k)}(\mathbf{r}_{(n,m-N_y)}) \, e^{i\Psi_{yb,4}} \tag{22}$$

$$\mathbf{F}_{4,add}^{(k)} = \Delta S_{xy} \mathbf{V}_{yb}^{(k)}(\mathbf{r}_{(n-N_x,m-N_y)}) \, e^{i\Psi_{yb,5}}. \tag{23}$$

8

The "phase" functions $\Psi_{yb,j}$, where $j = 1, \ldots, 5$, are defined as follows:

$$\Psi_{yb,1} = \mathbf{k} \cdot \left[\mathbf{r}_{(n,m)} - \mathbf{r}_{(n,m-1)} \right] \tag{24}$$

$$\Psi_{yb,2} = \mathbf{k} \cdot \left[\mathbf{r}_{(n,m)} - \mathbf{r}_{(n-1,m)} \right] \tag{25}$$

$$\Psi_{yb,3} = \mathbf{k} \cdot \left[\mathbf{r}_{(n-1,m)} - \mathbf{r}_{(n-1,m-1)} \right] \tag{26}$$

$$\Psi_{yb,4} = \mathbf{k} \cdot \left[\mathbf{r}_{(n,m)} - \mathbf{r}_{(n,m-N_y)} \right] \tag{27}$$

$$\Psi_{yb,5} = \mathbf{k} \cdot \left[\mathbf{r}_{(n-1,m)} - \mathbf{r}_{(n-N_x,m-N_y)} \right]. \tag{28}$$

To implement the 2-D FB/NSA algorithm associated with the y- expansion *efficiently*, it is required to store $\mathbf{F}_{yb}^{(k)}(\mathbf{r}_{(n,m)}, k_z, k_x)$ for each row associated with the weak region $S_{xy,yb}^f$; i.e. requiring an additional memory requirement of $\mathcal{O}(MQ_{TOT,y})$, where $Q_{TOT,y}$ is the total number of plane waves associated with the y- expansion. Thus, for the case of *extremely* large-scale 2-D rough surfaces with relatively large D_y the efficiency of the standard 2-D FB/NSA algorithm can be improved by incorporating the y- expansion, however the total memory requirement is increased as well.

After deforming the contours C_{k_z} and C_{k_x} to $C_{\delta_{k_z}}$ and $C_{\delta_{k_x}}$ respectively (see Figure 6 in [1] for $C_{\delta_{k_z}}$; $C_{\delta_{k_x}}$ is similar to $C_{\delta_{k_y}}$ as shown in Figure 7 in [1]), Eq. (13) can be discretized as follows:

$$\mathbf{J}_{w,yb}^{f,(k)}(\mathbf{r}) = -\frac{1}{4\pi^2} \Delta\Omega \sum_{u=-U}^{U} \sum_{v=-V_u}^{V_u} \frac{W(k_{z_u}, k_{x_v})[\mathbf{n} \times \mathbf{F}_{yb}^{(k)}(\mathbf{r}, k_{z_u}, k_{x_v})]}{k_{y_{u,v}}} e^{-i\delta_{k_z}} e^{-i\delta_{k_x}}, \tag{29}$$

where $k_{y_{u,v}} = (k^2 - k_{x_v}^2 - k_{z_u}^2)^{\frac{1}{2}}$, $W(k_{z_u}, k_{x_v})$ is a weighting function for numerical integration, $2U+1$ and $2V_u + 1$ are the number of plane waves in the complex k_z and k_x planes respectively, and δ_{k_z} and δ_{k_x} are the tilt angles of the deformed contours $C_{\delta_{k_z}}$ and $C_{\delta_{k_x}}$ with respect to the negative real axis. The total number of plane waves for y- expansion is given by

$$Q_{TOT,y} = \sum_{u=-U}^{U} (2V_u + 1). \tag{30}$$

Note that the topology in the complex k_z and k_x planes for the y- expansion is similar to the topology in the complex k_z and k_y planes for the x- expansion (see in [1, 3]), respectively. Thus, the 2-D NSA parameters associated with the y- expansion can be obtained using the same approach as employed in the x- expansion. Comparing the weak region $S_{xy,w}^f$ for the x- expansion and the weak region $S_{xy,yb}^f$ for the y- expansion with $y > y\prime$, it is observed that the 2-D NSA parameters for the y-expansion can be obtained from the corresponding 2-D NSA parameters for the x- expansion (see

9

in [1, 3]) by simply interchanging the following quantities: $L_x \to L_y, D_y \to L_x, k_y \to k_x, k_x \to k_y$ and $R_{xz} \to R_{yz}$. Thus, the 2-D NSA parameters in both complex k_z and k_x planes are given as:

$$\delta_{k_z} = \begin{cases} \frac{\pi}{4} & , \tan^{-1}\left(\frac{\Delta z_{max}}{L_y}\right) \le 0.1 \\ \tan^{-1}\beta & , \tan^{-1}\left(\frac{\Delta z_{max}}{L_y}\right) > 0.1 \end{cases} \tag{31}$$

$$k_{z,max} = \begin{cases} \sqrt{\frac{20k}{L_y}} & , \tan^{-1}\left(\frac{\Delta z_{max}}{L_y}\right) \le 0.1 \\ k_{z,s_{max}} + k_{z,tail} & , \tan^{-1}\left(\frac{\Delta z_{max}}{L_y}\right) > 0.1 \end{cases} \tag{32}$$

$$\Delta k_z = \frac{1}{22}\sqrt{\frac{C_z k}{L_y}} \tag{33}$$

$$\delta_{k_x} = \gamma \tag{34}$$

$$Re[k_{x,max}] = \begin{cases} \sqrt{\frac{20k}{L_y}} & , \tan^{-1}\left(\frac{L_x}{L_y}\right) \le 0.1 \\ Re[k_{x,s_{max}}] + k_{x,tail} & , \tan^{-1}\left(\frac{L_x}{L_y}\right) > 0.1 \end{cases} \tag{35}$$

$$\Delta k_x = \frac{1}{22}\sqrt{\frac{C_x k}{R_{xy}}}, \tag{36}$$

where $k_{z,s_{max}} = \frac{k\Delta z_{max}}{R_{yz}}$, $k_{x,s_{max}} = \frac{\kappa L_x}{R_{xy}}$, $\kappa = \left(k^2 - k_z^2\right)^{\frac{1}{2}}$, $R_{yz} = \sqrt{L_y^2 + (\Delta z_{max})^2}$, $R_{xy} = \sqrt{L_y^2 + L_x^2}$, and $\beta = \frac{1}{\max\{\xi,1\}}$, where ξ is the solution of the following nonlinear equation:

$$L_y\sqrt{\tau_1 - \tau_2} + \tau_3 = 0, \tag{37}$$

where $\tau_1 = 0.5\sqrt{4\tau_2^2 + \tau_4^2}$, $\tau_2 = 0.5\left[k^2(1+\xi)^2 + k_{z,s_{max}}^2(1-\xi^2)\right]$, $\tau_3 = (1+\xi)a_{max} - k_{z,s_{max}}\Delta z_{max}$, $\tau_4 = 2\xi k_{z,s_{max}}^2$, and a_{max} is some constant (typically found to be less than 3). Note that ξ can be solved numerically via a standard root-finding technique. In addition, there are six unknown constants in the above formulas: $\gamma, a_{max}, k_{z,tail}, k_{x,tail}, C_z$ and C_x, and these unknowns can be determined empirically by comparing the analytical solution of $g(\mathbf{r}, \mathbf{r}\prime)$ to the solution obtained from its spectral domain representation as discussed in detail in [1, 3].

The last issue associated with the y- expansion is that the radiation function $\mathbf{F}_{yb}^{(k)}(\mathbf{r}_{(n,m)}, k_z, k_x)$ can grow *geometrically* as the receiving element moves from left to right in the FS process. To see this, consider Eqs. (17), (19) and (20) with an observation that computing $\mathbf{F}_{yb}^{(k)}(\mathbf{r}_{(n,m)}, k_z, k_x)$ for $n > 1$ involves the previous calculated radiation function $\mathbf{F}_{yb}^{(k)}(\mathbf{r}_{(n-1,m)}, k_z, k_x)$ and the term $e^{i\Psi_{yb,2}}$. Note that $\Psi_{yb,2}$ defined in Eq. (25) can be simplified as follows:

$$\Psi_{yb,2} = k_x\Delta x + k_z\hat{z} \cdot \left[\mathbf{r}_{(n,m)} - \mathbf{r}_{(n-1,m)}\right]. \tag{38}$$

10

In general, the magnitude of the term $e^{i\Psi_{yb,2}}$ along the deformed contours $C_{\delta_{k_z}}$ and $C_{\delta_{k_x}}$ may be greater than, less than or equal to 1.0; i.e.

$$\left| e^{i\Psi_{yb,2}} \right| \gtreqless 1.0 \tag{39}$$

From Eq. (38), it is noted that $\Psi_{yb,2}$ does not involve the term $k_y\Delta y$, which typically assists in controlling $\left| e^{i\Psi_{yb,2}} \right|$ to be less than one. If $\left| e^{i\Psi_{yb,2}} \right| > 1.0$ along $C_{\delta_{k_z}}$ and $C_{\delta_{k_x}}$, as the receiving element moves from left to right, $\mathbf{F}_{yb}^{(k)}(\mathbf{r}_{(n,m)}, k_z, k_x)$ will grow geometrically since it involves a repeatedly multiplication process with $e^{i\Psi_{yb,2}}$. It should be pointed out that the above problem arises due to the fact that the NSA parameters for the y- expansion are chosen based on the two worst-case scenarios (i.e. one in the $\rho - z$ plane and another in the $x - y$ plane) as in the case of x- expansion [3]. The maximum of $x - x\prime$ employed in determining the NSA parameters in the complex k_x plane is equal to L_x. However, the weak region $S_{xy,yb}^{f}$ moves to the right with the approximate distance D_x, which is greater than the distance L_x employed in determining the NSA parameters, in the FS process. Note that the above problem can be avoided if the maximum of $x - x\prime$ is set to be D_x when determining the NSA parameters. However, the total number of plane waves $Q_{TOT,y}$ increases dramatically if using $\max\{x - x\prime\} = D_x$ since typically $D_x >> L_x$, and the efficiency of the NSA algorithm for the y- expansion degrades significantly.

One way to solve this problem is to *regenerate* the radiation function $\mathbf{F}_{yb}^{(k)}(\mathbf{r}_{(n,m)}, k_z, k_x)$ for a pre-specified horizontal distance L_r to stop the geometrically growing process before $\left| \mathbf{F}_{yb}^{(k)}(\mathbf{r}_{(n,m)}, k_z, k_x) \right|$ grows too large. The distance L_r can be determined by solving the following equation for N_r, where $L_r = N_r\Delta x$,

$$\text{Along } C_{\delta_{k_x}} : \qquad \chi^{N_r} = 10^{b_{max}} \tag{40}$$

or

$$\text{Along } C_{\delta_{k_x}} : \qquad N_r = \frac{b_{max}}{\log \chi}, \tag{41}$$

where χ is the maximum of $\left| e^{ik_x\Delta x} \right|$ and b_{max} is a given positive constant. Typically, $b_{max} \in [4.0, 6.0]$ yields accurate results with an appropriate value for L_r. After $\mathbf{F}_{yb}^{(k)}(\mathbf{r}_{(n,m)}, k_z, k_x)$ is generated, it can be computed recursively again using Eqs. (17) to (28) until it is regenerated for the next L_r. This process continues until the receiving element reaches the final (N, M) th element on the surface S.

For the NSA algorithm using the x- expansion in [1], it should be pointed out that the radiation function $\mathbf{F}^{(k)}(\mathbf{r}_{(n,m)}, k_z, k_y)$ (see Eq. (19) in [1]) does *not* grow up too large as the receiving element moves in the y- direction from bottom to top in the FS process. The reason for this is that the maximum of $|y - y\prime|$ employed in determining the NSA parameters in the complex k_y plane is equal to D_y, which is equal to the maximum vertical distance D_y that the receiving element can move in the FS process; i.e. the NSA parameters for the x- expansion are chosen appropriately. Thus, it is *not* necessary to regenerate $\mathbf{F}^{(k)}(\mathbf{r}_{(n,m)}, k_z, k_y)$ for the x- expansion.

As discussed earlier, the NSA algorithm associated with $\mathbf{J}_{w,yt}^{f,(k)}(\mathbf{r})$ for $y < y\prime$ can be formulated in a similar fashion as the NSA algorithm associated with $\mathbf{J}_{w,yb}^{f,(k)}(\mathbf{r})$ for $y > y\prime$. However, it should be pointed out that the radiation function $\mathbf{F}_{yt}^{(k)}(\mathbf{r}_{(n,m)}, k_z, k_x)$ associated with $\mathbf{J}_{w,yt}^{f,(k)}(\mathbf{r})$ must be computed recursively in an *increasing* manner of the weak region $S_{xy,yt}^{f}$ otherwise $\mathbf{F}_{yt}^{(k)}(\mathbf{r}_{(n,m)}, k_z, k_x)$ will grow *geometrically*. For example, for the middle column of Figure 4, $\mathbf{F}_{yt}^{(k)}(\mathbf{r}_{(n,m)}, k_z, k_x)$ is computed recursively by starting at Figure 4 (m) and ending with Figure 4 (k). Like $\mathbf{F}_{yb}^{(k)}(\mathbf{r}_{(n,m)}, k_z, k_x)$ for $y > y\prime$, $\mathbf{F}_{yt}^{(k)}(\mathbf{r}_{(n,m)}, k_z, k_x)$ is also regenerated for every horizontal distance L_r. It should be pointed out that it is straight forward to extend the above formulation for impedance surfaces [2]. Finally, numerical results in Section 5.1 will illustrate that the NSA algorithm employing both x- and y- expansions yields *less* CPU requirements than the one using the x- expansion for the case of relatively large D_y. In the next section, the 2-D "multilevel" FB/NSA algorithm for *extremely* large-scale surfaces is illustrated.

3   The 2-D "Multilevel" FB/NSA Algorithm for Extremely Large-Scale Surfaces

For 2-D *extremely* large-scale surfaces, the NSA parameters for the x- expansion given in [1] may yield inaccurate results for a pair of source and observation points where $x - x\prime \gg L_x$. Like the 1-D NSA algorithm [4], this problem can be solved by decomposing the *old* weak region $S_{xy,w}^{f}$ (see Figure 2) into more than one weak region as shown in Figure 3 for the FS direction. For 1-D *extremely* large-scale surfaces [4], it is found that only a *few* weak region (or even one) are usually required for most practical problems to obtain the desired accuracy due to the fact that

contributions from other far-away weak regions are *negligible* compared to those for the first few regions. Thus, it is expected that only a few weak regions are required for most practical 2-D extremely large-scale surface problems as well.

Due to mathematical complexity, it is difficult to determine the appropriate sizes of the weak regions $S_{xy,w}^{f,j}$ *analytically*, where $j = 1, \ldots, T$ and T is the total number of the weak regions for a given surface size, however the appropriate size of each weak region can be determined *empirically*. To illustrate the above concept, consider the *first* weak region $S_{xy,w}^{f,1}$. The horizontal distance $L_{w,1}$ of $S_{xy,w}^{f,1}$ is chosen such that the relative error obtained from computing the scalar Green's function $g(\mathbf{r}, \mathbf{r}\prime)$ using the exact expression (see Eq. (2)) and the spectral integral representation in the x-direction (see Eq. (20) in [1]), for the case of $x - x\prime = L_x + L_{w,1}, y - y\prime = D_y$ and $\Delta z = \Delta z_{max}$, is less than a specified tolerance, which is typically set to be 5.0%. In other words, the horizontal distance $L_{w,1}$ is adjusted, when the variations of the source and observation points in the y- and z-directions are maximum, such that the relative error satisfies a specified tolerance. In the first weak region $S_{xy,w}^{f,1}$, it should be pointed out that the 2-D NSA parameters are *fixed* before the horizontal distance $L_{w,1}$ is determined by studying the scalar Green's function $g(\mathbf{r}, \mathbf{r}\prime)$ for a pair of source and observation points in the two worst-case scenarios (i.e. one in the $\rho - z$ plane and another in the $x - y$ plane) as discussed in [3]. Once $L_{w,1}$ is known, the 2-D NSA parameters employed in the *second* weak region $S_{xy,w}^{f,2}$ can be determined empirically by following the same approach as for the *first* weak region. Note that the *effective* strong distance employed in the calculation of the 2-D NSA parameters in $S_{xy,w}^{f,2}$ is equal to $L_x + L_{w,1}$. This process continues until the sum of the neighborhood distance L_x and all weak-region horizontal distances exceeds the along-range surface size D_x. Numerical results in Section 5.2 confirm that the accuracy of the standard 2-D FB/NSA algorithm (using only x- expansion) is improved when incorporating the "multilevel" algorithm for the case of *extremely* large-scale surfaces. In the next section, the computational cost and memory storage requirements of the FB/NSA method for 2-D RSS problems are discussed.

4   Computational Cost and Memory Storage Requirement of the 2-D FB/NSA Method

The total operational count TOC of the 2-D "multilevel" FB/NSA method using both x- and y-expansions is estimated as follows:

$$TOC \sim C_r N_{s,r} N_{elmt} + C_y Q_{TOT,y} N_{elmt} + \sum_{j=1}^{T} C_j Q_{TOT,x,j}(N_{elmt} - N_{s,j}), \tag{42}$$

where $N_{s,r} = 2N_x N_y, N_{elmt} = NM = 0.5 N_{tot}, Q_{TOT,y}$ denotes the total number of plane waves for the y- expansion as defined in Eq. (30), $Q_{TOT,x,j}$ denotes the total number of plane waves for the x- expansion employed in the j th weak region $S_{xy,w}^{f,j}$, where $j = 1, \ldots, T$, C_j are constants, and

$$N_{s,j} = \left(N_x + \sum_{m=1}^{j-1} N_{w,m} \right) M, \qquad j = 2, \ldots, T, \tag{43}$$

where $N_{s,1} = N_x M$ and $N_{w,m} = \frac{L_{w,m}}{\Delta x}$, where $L_{w,m}$ is the horizontal distance of the m th weak region $S_{xy,w}^{f,m}$ and $m = 1, \ldots, T-1$. It is noted that $N_{s,r}$ is approximately the total number of elements in the reduced strong region $S_{xy,rs}^{f}$. The first term on the RHS of Eq. (42) is the number of operations involved in the computation of the reduced strong-region contribution for N_{elmt} receiving elements and the second term involves the number of operation count to compute $Q_{TOT,y}$ plane waves associated with $\mathbf{J}_{w,yb}^{f,(k)}(\mathbf{r})$ and $\mathbf{J}_{w,yt}^{f,(k)}(\mathbf{r})$ for N_{elmt} receiving elements. Note that the operational count of the regeneration process of complex vector radiation functions $\mathbf{F}_{yb}^{(k)}(\mathbf{r}_{(n,m)}, k_z, k_x)$ and $\mathbf{F}_{yt}^{(k)}(\mathbf{r}_{(n,m)}, k_z, k_x)$ for every horizontal distance L_r (see Eq. (41) is proportional to N_{elmt}. Finally, the last term is the number of operations involved in the computation of $Q_{TOT,x,j}$ plane waves associated with the j th weak region $S_{xy,w}^{f,j}$.

In addition, the total memory storage requirement $TMSR$ of the 2-D "multilevel" FB/NSA algorithm using both x- and y- expansions can be estimated as follows:

$$TMSR \sim C_w N_{elmt} + C_m M Q_{TOT,y} + \sum_{j=1}^{T} D_j Q_{TOT,x,j}, \tag{44}$$

where C_j and D_j are constants. The first term on the RHS of Eq. (44) accounts for the storage of necessary matrices and vectors employed in the 2-D "multilevel" FB/NSA algorithm using both x- and y- expansions. In addition, the second and third terms involve the storage of the total

number of plane waves associated with the y- expansion and the x- expansions employed in the "multilevel" algorithm, respectively. As pointed out earlier in Section 2, to implement the 2-D FB/NSA algorithm associated with the y- expansion *efficiently*, it is required to store the number of plane waves for each row associated with the weak regions $S^f_{xy,yb}$ and $S^f_{xy,yt}$ resulting in an additional memory requirement of $\mathcal{O}(MQ_{TOT,y})$.

In practice, it should be pointed out that only *few* weak regions $S^{f,j}_{xy,w}$ are *sufficient* to yield accurate results for 2-D *extremely* large-scale surfaces as in the case of 1-D surfaces [4]. Note that the neighborhood distances L_x and L_y must be chosen appropriately to compromise between the direct computation in the strong region and the NSA computation in the weak regions. However, for fixed D_y, frequency and surface roughness, the parameters $L_x, L_y, Q_{TOT,x,j}$ and $Q_{TOT,y}$ are fixed, and as D_x increases it is implied from Eqs. (42) and (44) that the computational cost and memory storage requirement of the 2-D "multilevel" FB/NSA algorithm using both x- and y- expansions remain $\mathcal{O}(N_{tot})$. Finally, it should be emphasized that the 2-D "multilevel" FB/NSA algorithm using both x- and y- expansions improves the efficiency and accuracy of the standard 2-D FB/NSA algorithm using only the x- expansion at the cost of increasing memory storage requirements and algorithmic complexity.

5   Numerical Results

In this section, several numerical results of rough surface scattering computed by the 2-D FB/NSA algorithm are illustrated. Numerical results are presented in terms of the normalized bistatic radar cross section (RCS) $\sigma_{\alpha\beta}(\theta_s, \phi_s)$ in the plane of incidence, defined for a scattered wave in α-polarization and an incident wave in β-polarization (see Eq. (34) in [1]). For rough surfaces with *relatively large* D_y, it is recommended to employ the 2-D FB/NSA algorithm using both x- and y- expansions as described in Section 2, and its results are presented in Section 5.1. The 2-D "multilevel" FB/NSA algorithm is suitable for *extremely* large-scale surfaces, and its numerical results are illustrated in Section 5.2. Note that the information of the CPU time in this section is based on a Pentium II 200 MHz computer with 256 Mbytes RAM.

15

5.1 The 2-D FB/NSA Algorithm Using Both x- and y- Expansions

To illustrate the computational efficiency and accuracy of the 2-D FB/NSA algorithm using both x- and y- expansions for large-scale surfaces with relatively large D_y, consider a *deterministic* $128\lambda \times 32\lambda$ PEC rough surface sampled with 16 points per λ resulting in $2,097,152$ unknowns, where λ is the electromagnetic wavelength in free space.

The surface is illuminated by a tapered plane wave with $g\prime = 6$ [5] at an incident angle of $80°$. The surface is a realization of a Gaussian random process described by a power law spectrum,

$$W(k,\phi) = a_0 k^{-4}, \quad k_{dl} < k < k_{du}, \tag{45}$$

where $W(k,\phi)$ represents the spectral amplitude, k denotes the spatial wave number of the surface, ϕ represents the azimuthal angle of the two dimensional spectrum, a_0 is a specified constant, and k_{dl} and k_{du} are the lower and upper cutoff spatial wave numbers, respectively. The surface spectrum parameters of interest are $a_0 = 0.6365 \times 10^{-3}$, $k_{dl} = 210.0$ rad./λ and $k_{du} = 27,393.3$ rad./λ, and its maximum surface variation Δz_{max} is equal to 1.6435λ ($z_{min} = -0.8311\lambda$ and $z_{max} = 0.8124\lambda$). In this case, numerical tests show that only the first weak region $S_{xy,w}^{f,1}$ employed for the x- expansion is sufficient to yield accurate results. The 2-D FB/NSA parameters for this case are listed below (see the definitions of the 2-D NSA parameters for the x- expansion in [1]):

- For the x- expansion: $L_x = 3.0\lambda$, $\delta_{k_y} = 0.03$ rad., $a_{max} = 1.0$, $k_{z,tail} = 0.60k$,

$$k_{y,tail} = 0.25 \ Re[\kappa], \ C_z = 30.0, \ C_y = 11.0, \ Q_{TOT,x,1} = 8,971$$

- For the y- expansion: $L_y = 3.0\lambda$, $\delta_{k_x} = 0.3$ rad., $a_{max} = 1.0$, $b_{max} = 4.0$, $k_{z,tail} = 0.60k$,

$$k_{x,tail} = 0.30 \ Re[\kappa], \ C_z = 40.0, \ C_x = 40.0, \ Q_{TOT,y} = 1,305$$

Note that the y- expansion employs $b_{max} = 4.0$, and from Eq. (41) it is required to regenerate the radiation function $\mathbf{F}_{yb}^{(k)}(\mathbf{r}_{(n,m)}, k_z, k_x)$ for every 75 points (i.e. $L_r = 4.6875\lambda$). The standard 2-D FB/NSA algorithm using the x- expansion is employed to compare with the 2-D FB/NSA algorithm using both x- and y- expansions, and the former employs the same 2-D NSA parameters as the latter for the x- expansion. It is found that both methods require only 2 iterations to converge to within 1% accuracy based on the normalized pseudo-residual test [1]. Figure 5 (a) and (b) illustrates plots of the normalized bistatic RCS in dB when $\phi_i = \phi_s = 0°$ versus the scattering angle θ_s for HH-

and VH- polarizations respectively, comparing between the former and the latter. From the plots, the results obtained from both methods are in excellent agreement. The former requires the total CPU time of $21,622.5$ minutes, and the latter's CPU time is equal to $13,755.3$ minutes. Thus, it is obvious that the latter provides very accurate results, and the former's efficiency can be indeed improved by incorporating the y- expansion.

To further verify the computational efficiency and accuracy of the 2-D FB/NSA algorithm using both x- and y- expansions, consider another *deterministic* $64\lambda \times 64\lambda$ *square* PEC rough surface sampled with 8 points per λ resulting in $524,288$ unknowns. The surface is illuminated by a tapered plane wave with $g\prime = 6$ at an incident angle of $40°$. Same surface statistics as in the above example are employed in this case, and its maximum surface variation Δz_{max} is equal to 1.9115λ ($z_{min} = -0.9377\lambda$ and $z_{max} = 0.9738\lambda$). Numerical tests show that only the first weak region $S_{xy,w}^{f,1}$ employed for the x- expansion is sufficient to yield accurate results. The 2-D FB/NSA parameters for this case are listed below:

- For the x- expansion: $L_x = 6.0\lambda$, $\delta_{k_y} = 0.02$ rad., $a_{max} = 2.0$, $k_{z,tail} = 0.05k$,

$$k_{y,tail} = 0.04\, Re[\kappa],\ C_z = 45.0,\ C_y = 7.0,\ Q_{TOT,x,1} = 5,933$$

- For the y- expansion: $L_y = 3.0\lambda$, $\delta_{k_x} = 0.1$ rad., $a_{max} = 2.0$, $b_{max} = 4.0$, $k_{z,tail} = 0.05k$,

$$k_{x,tail} = 0.20\, Re[\kappa],\ C_z = 35.0,\ C_x = 15.0,\ Q_{TOT,y} = 1,747$$

Note that the y- expansion employs $b_{max} = 4.0$, and from Eq. (41) it is required to regenerate the radiation function $\mathbf{F}_{yb}^{(k)}(\mathbf{r}_{(n,m)}, k_z, k_x)$ for every 103 points (i.e. $L_r = 12.875\lambda$). Figure 6 (a) and (b) plots the normalized bistatic RCS in dB when $\phi_i = \phi_s = 0°$ versus the scattering angle θ_s for HH- and VH- polarizations respectively, comparing between the 2-D FB/NSA algorithm using only the x- expansion and the one using both x- and y- expansions. Both methods require only 2 iterations to converge to within 1% accuracy based on the normalized pseudo-residual test [1]. From the plots, the results obtained from both methods are in excellent agreement. The former requires the total CPU time of $4,816.4$ minutes, and the latter's CPU time is equal to $2,848.2$ minutes. Thus, it can be concluded that incorporating the y- expansion assists in improving the computational efficiency of the standard 2-D FB/NSA algorithm without degrading its accuracy for rough surfaces with *relatively large D_y*. It should be pointed out that the y- expansion shows better improvement for

larger problems with *relatively large* D_y as can be seen from the above two examples. In the next section, numerical results of the 2-D "multilevel" FB/NSA algorithm are illustrated.

5.2 The 2-D "Multilevel" FB/NSA Algorithm

To see that the "multilevel" algorithm can improve the accuracy of the standard (one-level) 2-D FB/NSA algorithm, consider a *deterministic* $256\lambda \times 32\lambda$ PEC rough surface sampled with 8 points per λ resulting in $1,048,576$ unknowns. The surface is a realization of a Gaussian random process described by a power law spectrum defined in Eq. (45) with $a_0 = 0.6365 \times 10^{-3}$, $k_{dl} = 210.0$ rad./λ and $k_{du} = 27,393.3$ rad./λ, and its maximum surface variation Δz_{max} is equal to 2.361λ ($z_{min} = -1.359\lambda$ and $z_{max} = 1.002\lambda$). The surface is illuminated by a tapered plane wave with $g\prime = 6$ [5] at an incident angle of $80°$. The 2-D *two-level* FB/NSA parameters using only the x-expansion for this case are given as follows:

- The *first* level: $L_x = 3.0\lambda$, $L_{w,1} = 50.0\lambda$, $\delta_{k_y} = 0.03$ rad., $a_{max} = 1.0$, $k_{z,tail} = 0.45k$,

$$k_{y,tail} = 0.20\ Re[\kappa],\ C_z = 25.0,\ C_y = 11.0,\ Q_{TOT,x,1} = 8,473$$

- The *second* level: $L_x + L_{w,1} = 53.0\lambda$, $\delta_{k_y} = 0.20$ rad., $a_{max} = 1.0$, $k_{z,tail} = 0.20k$,

$$k_{y,tail} = 0.10\ Re[\kappa],\ C_z = 30.0,\ C_y = 15.0,\ Q_{TOT,x,2} = 5,217$$

It is found that the 2-D two-level FB/NSA algorithm requires only 2 iterations to converge to within 1% accuracy based on the normalized pseudo-residual test [1]. The sparse-matrix canonical grid (SMCG) method [8] is employed to compare with the 2-D FB/NSA algorithm. Figure 7 (a) and (b) shows plots of the normalized bistatic RCS in dB when $\phi_i = \phi_s = 0°$ versus θ_s for HH- and VH-polarizations respectively, comparing between the 2-D two-level FB/NSA algorithm and the SMCG method. Note that the results obtained from both methods are in good agreement. In addition, Figure 8 illustrates the same plots as in Figure 7, but comparing between the 2-D *one-level* FB/NSA method and the SMCG method. It is found that the 2-D *one-level* FB/NSA method requires 2 iterations as well as the 2-D *two-level* FB/NSA method. From the plots, the discrepancy of the results obtained from the 2-D *one-level* FB/NSA method and the SMCG method is noticeable. Note that the 2-D one-level and two-level FB/NSA methods require the total CPU time of 4994.1

and 8327.2 minutes, respectively. Thus, the "multilevel" algorithm can indeed improve the accuracy of the 2-D one-level FB/NSA algorithm at the cost of increasing the total CPU time.

6 Conclusions

The FB/NSA method has been shown to be an efficient $\mathcal{O}(N_{tot})$ method for 2-D *large-scale* rough surfaces with *moderate* surface cross-range size D_y. For rough surfaces with *relatively large* D_y, it is more efficient to employ the 2-D FB/NSA algorithm using both x- and y- expansions. The y-expansion is employed to reduce the computational complexity of the *large* strong region $S_{xy,s}^f$, and it can be formulated in a similar fashion as the x- expansion. Note that the 2-D FB/NSA algorithm using both x- and y- expansions requires an additional memory storage of $\mathcal{O}(MQ_{TOT,y})$ compared to the standard 2-D FB/NSA algorithm using only the x- expansion. Numerical results illustrate that incorporating the y- expansion to the standard 2-D FB/NSA algorithm can indeed improve its computational efficiency without degrading its accuracy.

For *extremely* large-scale surfaces, the 2-D "multilevel" FB/NSA algorithm is employed to improve the accuracy of the original (one-level) 2-D FB/NSA algorithm, however the "multilevel" algorithm increases both total CPU time and memory storage requirement. Only a *few* weak regions are sufficient to obtain accurate results for most practical 2-D *extremely* large-scale surface problems. For given surface sizes and surface statistics, it is *difficult* to determine the appropriate sizes of the weak regions $S_{xy,w}^{f,j}$ *analytically*, but they can be found *empirically* instead. It is emphasized that the 2-D NSA parameters for the x- expansion must be determined appropriately for each weak region as well. Numerical results show that the "multilevel" algorithm can indeed improve the accuracy of the one-level 2-D FB/NSA algorithm at the cost of increasing the total CPU time and memory storage requirement. Finally, the computational efficiency of the *improved* FB/NSA method for 2-D *extremely* large-scale surfaces with *relatively large* D_y remains $\mathcal{O}(N_{tot})$ for fixed D_y, frequency and surface roughness.

References

[1] D. Torrungrueng, H.-T. Chou and J. T. Johnson, "A Novel Acceleration Algorithm for the Computation of Scattering from Two-Dimensional Large-Scale Perfectly Conducting Random Rough Surfaces with the Forward-Backward Method ," *IEEE Trans. Geosci. Rem. Sens.*, Vol. 38, pp. 1656–1668, 2000.

[2] D. Torrungrueng and J. T. Johnson, "The Forward-Backward Method with a Novel Acceleration Algorithm (FB/NSA) for the Computation of Scattering from Two-Dimensional Large-Scale Impedance Random Rough Surfaces," *submitted to Micro. Opt. Tech. Lett.*.

[3] D. Torrungrueng, *Applications of the Novel Spectral Acceleration (NSA) Algorithm for the Computation of Scattering from Rough Surfaces*, Ph.D. Dissertation, The Ohio State University, Columbus, OH, 2000.

[4] D. Torrungrueng, J. T. Johnson and H.-T. Chou, "Some Issues Related to the Novel Spectral Acceleration (NSA) Method for the Fast Computation of Radiation/Scattering from One-Dimensional *Extremely* Large-Scale Quasi-Planar Structures," *submitted to Radio Science.*

[5] J. T. Johnson, L. Tsang, R. T. Shin, K. Pak, C. H. Chan, A. Ishimaru and Y. Kuga, "Backscattering Enhancement of Electromagnetic Waves from Two-Dimensional Perfectly Conducting Random Rough Surfaces: A Comparison of Monte Carlo Simulations with Experimental Data," *IEEE Trans. Antennas Prop.*, Vol. 44, pp. 748–756, 1996.

[6] J. T. Johnson, R. T. Shin, J. A. Kong, L. Tsang and K. Pak, "A Numerical Study of Ocean Polarimetric Thermal Emission," *IEEE Trans. Geosci. Rem. Sens.*, Vol. 37, pp. 8–20, 1999.

[7] R. F. Harrington, *Field Computation by Moment Methods*, Krieger, Wiley, Malarbar FL, 1982.

[8] K. Pak, L. Tsang and J. T. Johnson, "Numerical simulations and Backscattering Enhancement of Electromagnetic Waves from Two-Dimensional Dielectric Random Rough Surfaces with the Sparse-Matrix Canonical Grid Method," *J. Opt. Soc. Am. A*, Vol. 14, pp. 1515–1529, 1997.
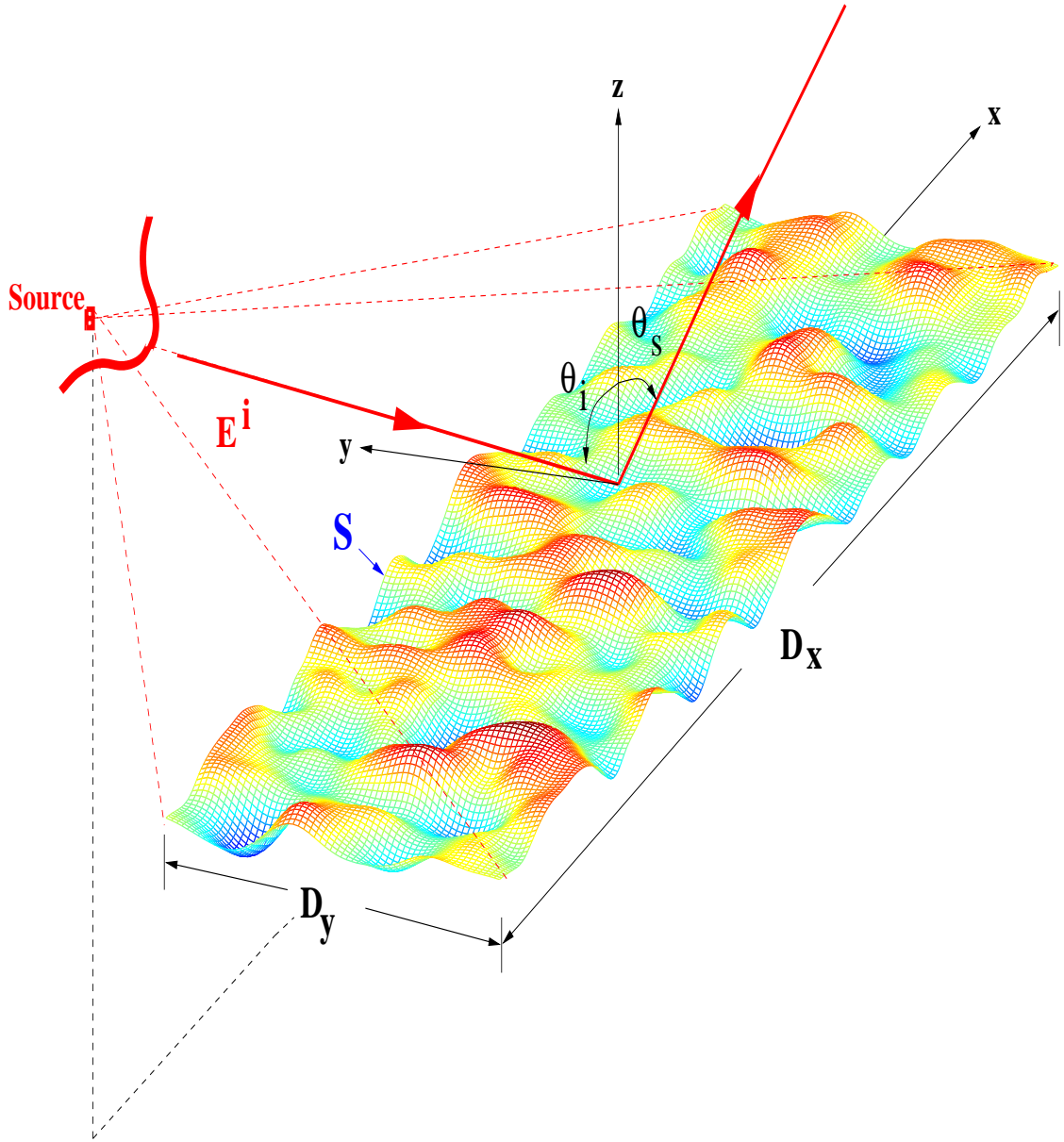
Figure 1: A 2-D PEC rough surface profile S illuminated by a *tapered* incident field $\mathbf{E}^i(x, y, z)$ centered at the origin and propagating in direction $\hat{k}_i = \hat{x} \sin \theta_i \cos \phi_i + \hat{y} \sin \theta_i \sin \phi_i - \hat{z} \cos \theta_i$.
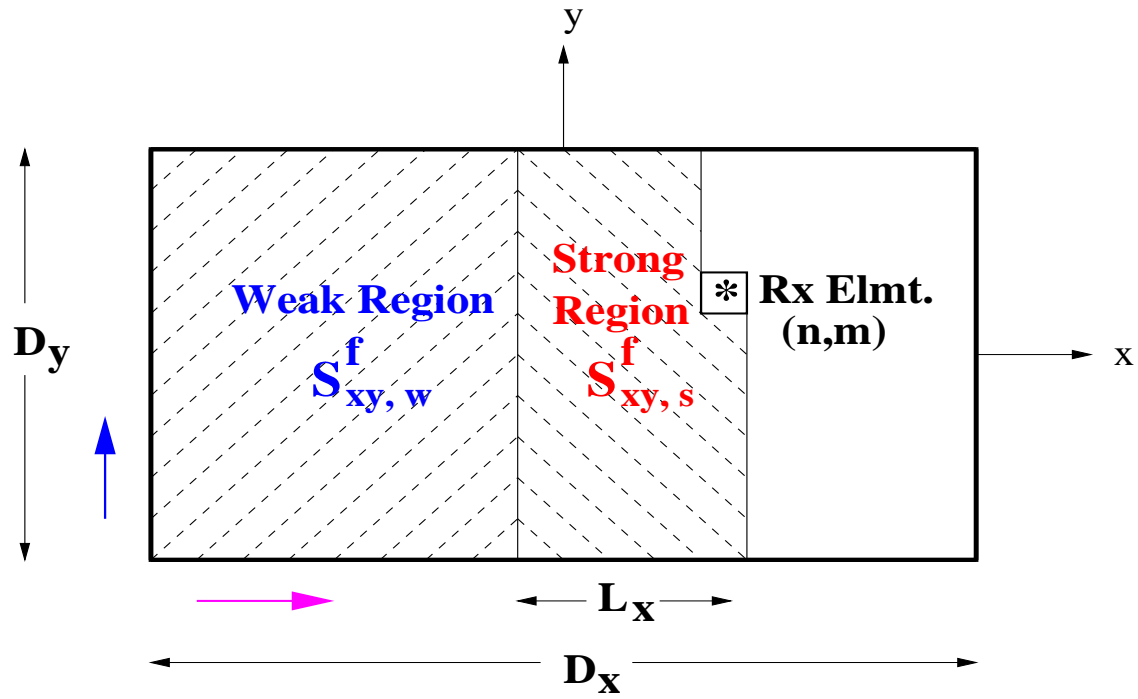
Figure 2: Strong and weak regions in the FS direction.
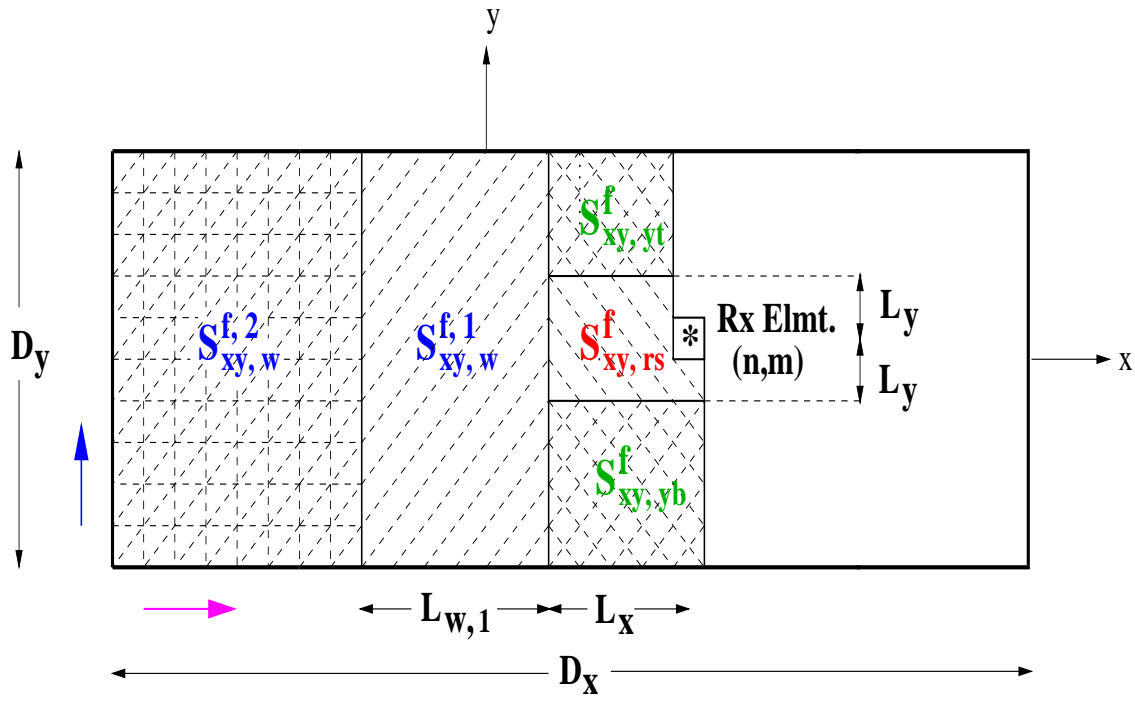
Figure 3: Decomposition of regions in the FS direction for extremely large-scale 2-D RSS problems.
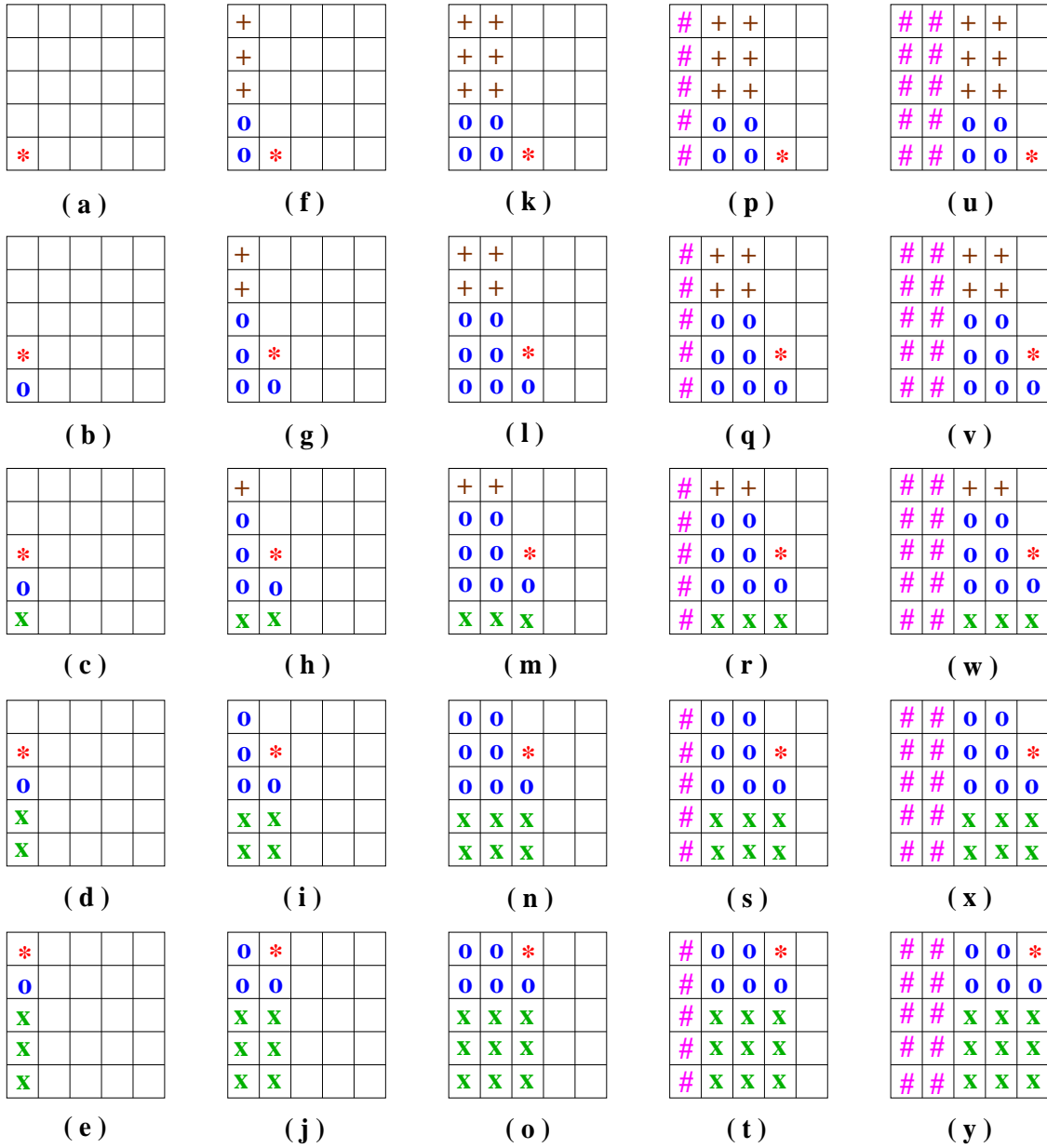
Figure 4: The FS process in the 2-D FB/NSA algorithm using both x- and y- expansions with the following parameters: $N = 5, M = 5, N_x = 3$ and $N_y = 2$.
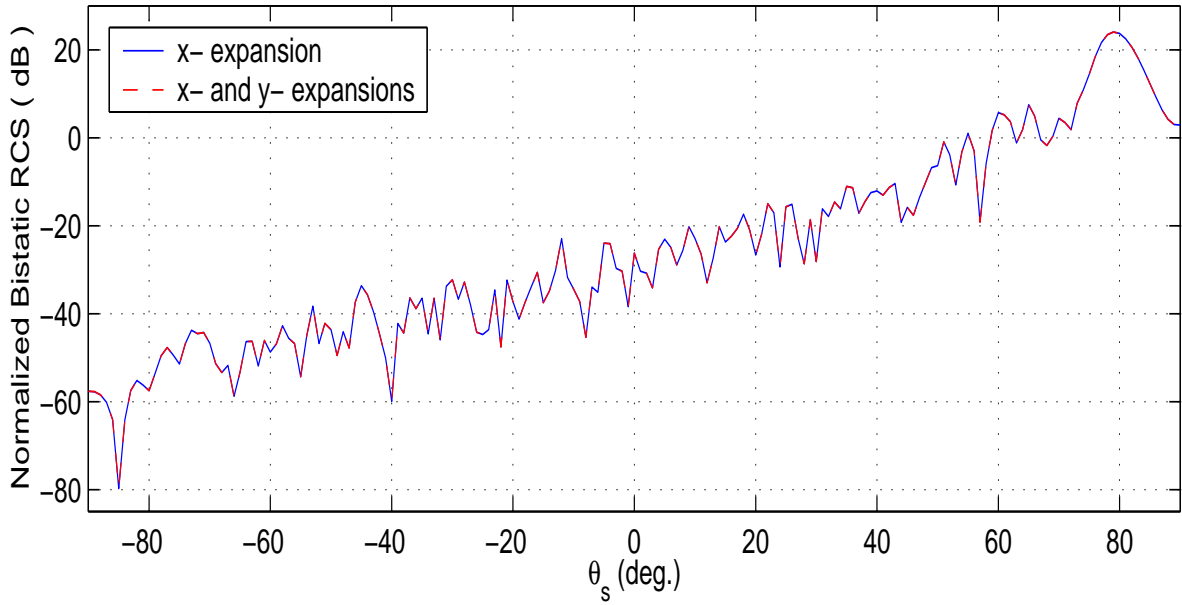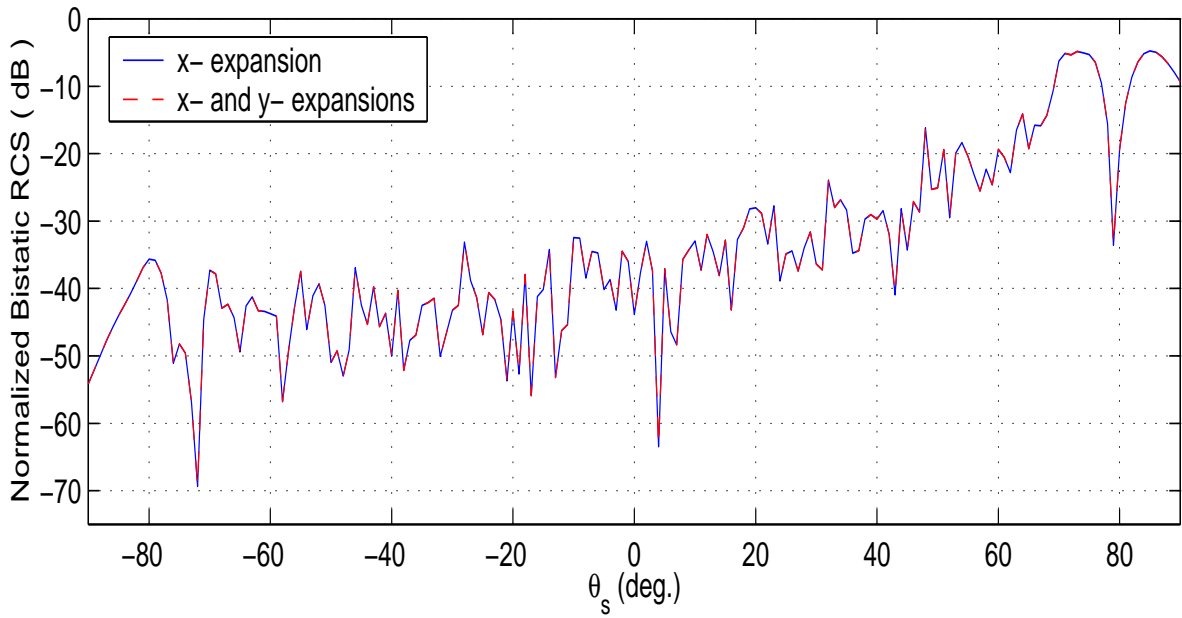
Figure 5: A comparison of the normalized bistatic RCS in dB when $\phi_i = \phi_s = 0°$ for a *rectangular* rough surface computed by the standard 2-D FB/NSA algorithm using the x- expansion and the one using both x- and y- expansions: (a) HH polarization (b) VH polarization.
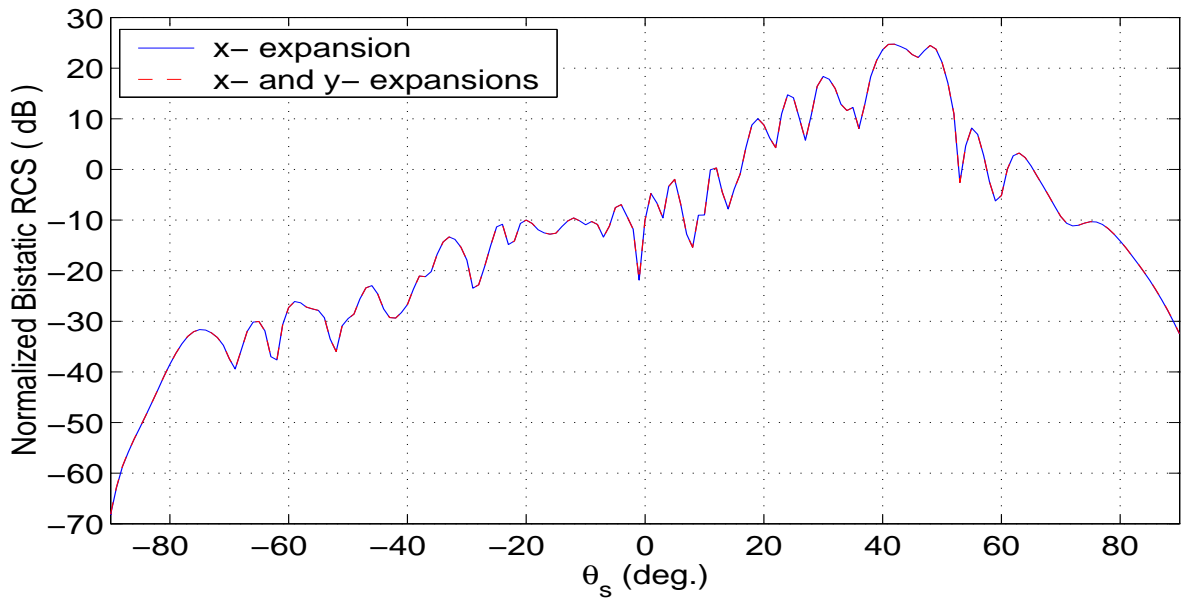
(a)
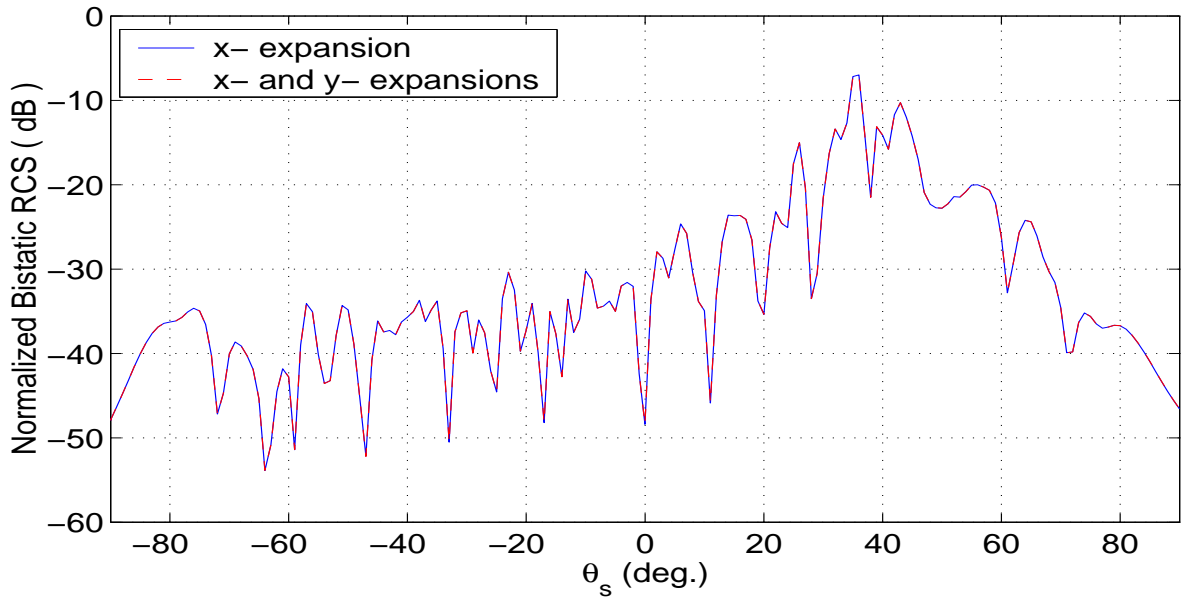
(b)

Figure 6: A comparison of the normalized bistatic RCS in dB when $\phi_i = \phi_s = 0°$ for a *square* rough surface computed by the standard 2-D FB/NSA algorithm using the x- expansion and the one using both x- and y- expansions: (a) HH polarization (b) VH polarization.
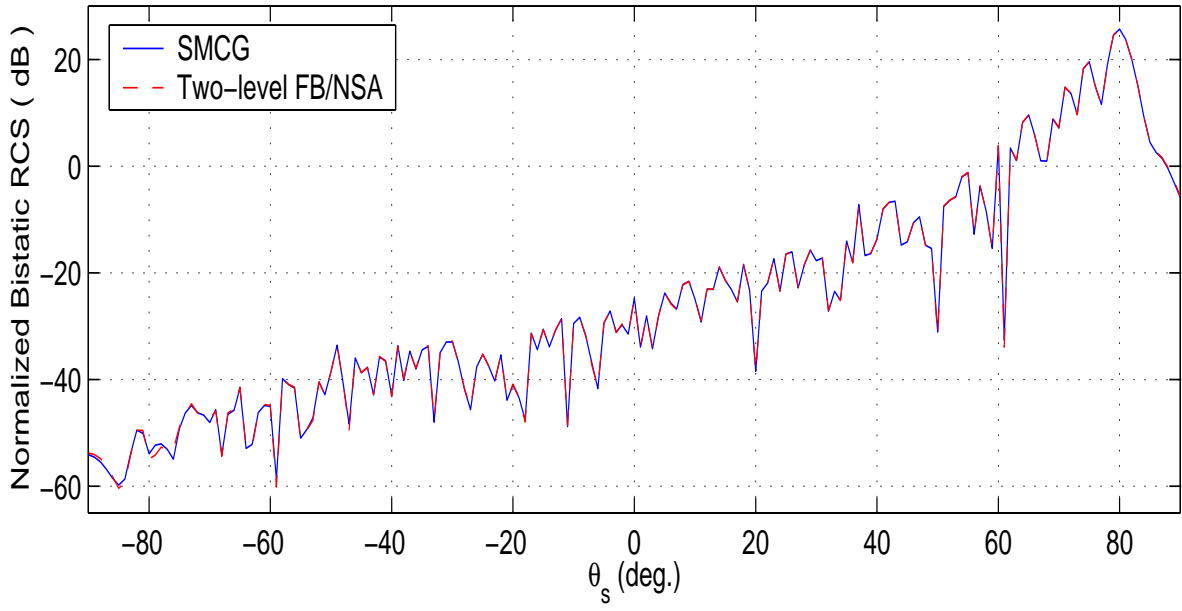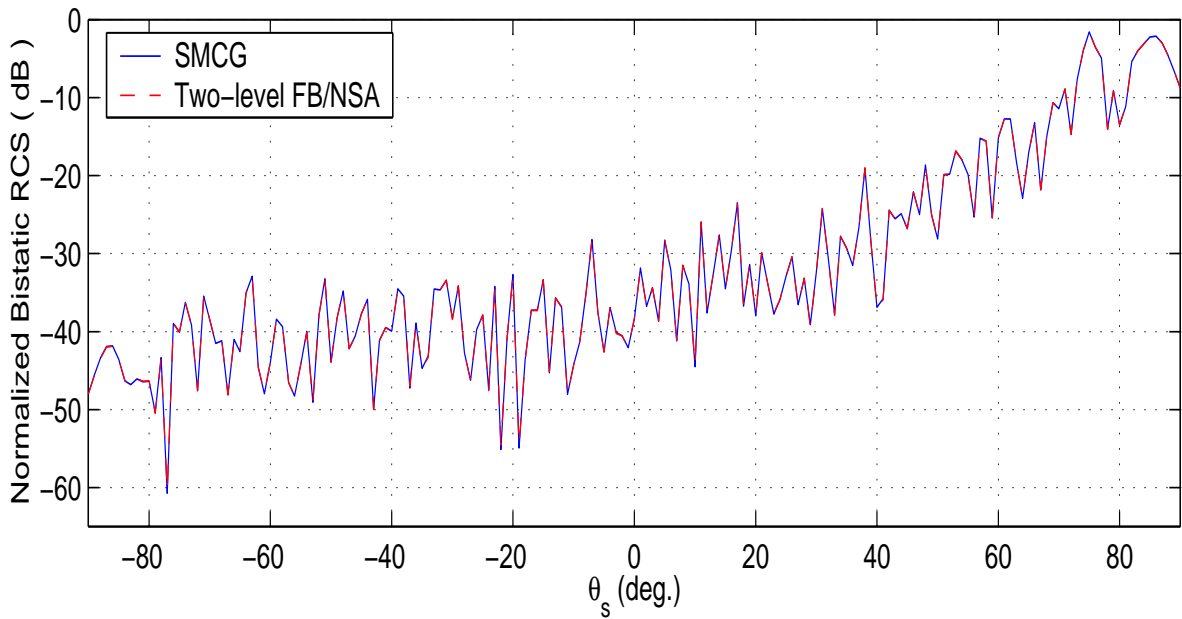
Figure 7: A comparison of the normalized bistatic RCS in dB when $\phi_i = \phi_s = 0°$ computed by the 2-D *two-level* FB/NSA method and the SMCG method: (a) HH polarization (b) VH polarization.
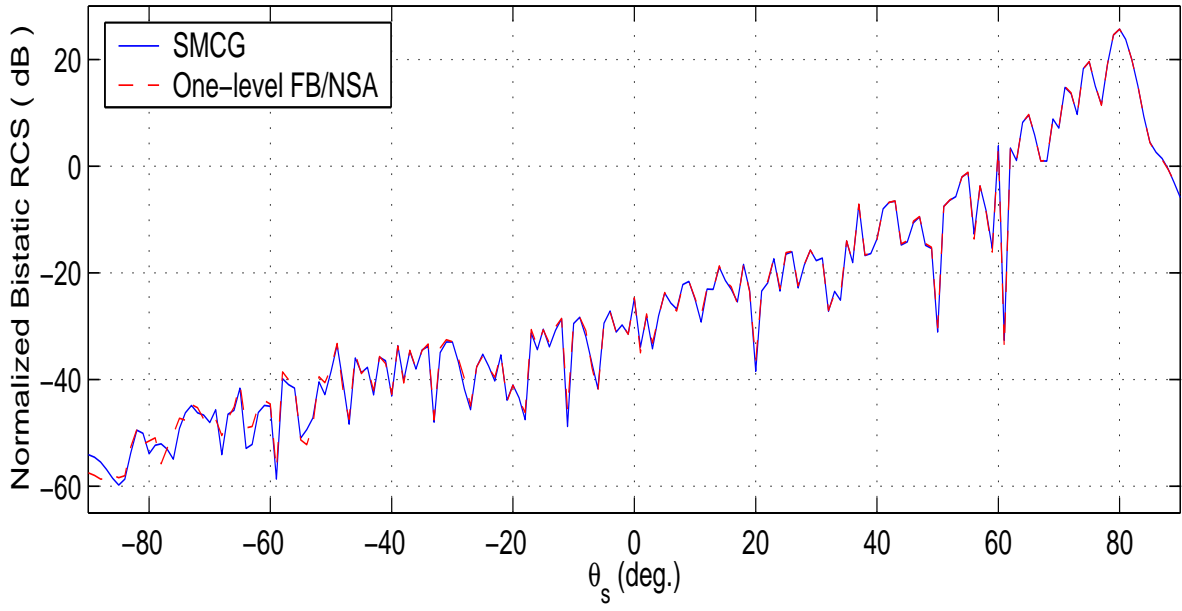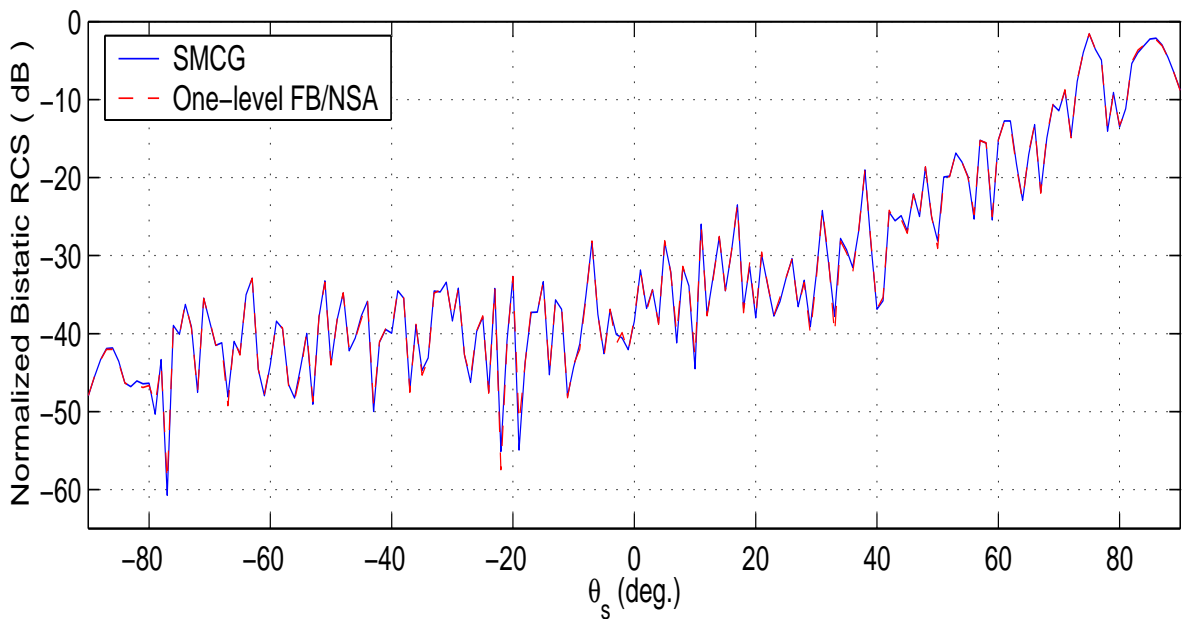
Figure 8: A comparison of the normalized bistatic RCS in dB when $\phi_i = \phi_s = 0°$ computed by the 2-D *one-level* FB/NSA method and the SMCG method: (a) HH polarization (b) VH polarization.